Chemical Science

EDGE ARTICLE

View Article Online
View Journal | View Issue

Cite this: *Chem. Sci.*, 2018, **9**, 7809

All publication charges for this article have been paid for by the Royal Society of Chemistry

Understanding complex supramolecular landscapes: non-covalent macrocyclization equilibria examined by fluorescence resonance energy transfer†

María J. Mayoral,*[a] David Serrano-Molina,[a] Jorge Camacho-García,[a] Eva Magdalena-Estirado,[a] Marina Blanco-Lomas,[a] Elham Fadaei[a] and David González-Rodríguez*[ab]

Received 20th July 2018
Accepted 16th August 2018

DOI: 10.1039/c8sc03229g

rsc.li/chemical-science

As molecular self-assembled systems increase in complexity, due to a large number of participating entities and/or the establishment of multiple competing equilibria, their full understanding becomes likewise more complicated, and the use of diverse analytical techniques that can afford complementary information is required. We demonstrate in this work that resonance excitation energy transfer phenomena, measured by fluorescence spectroscopy in combination with other optical spectroscopies, can be a valuable tool to obtain supplementary thermodynamic data about complex supramolecular landscapes that other methods fail to provide. In particular, noncovalent macrocyclization processes of lipophilic dinucleosides are studied here by setting up a competition between intra- and intermolecular association processes of Watson–Crick H-bonding pairs. Multiwavelength analysis of the monomer emission changes allowed us to determine cyclotetramerization constants and to quantify chelate cooperativity, which was confirmed to be substantially larger for the G-C than for the A-U pair. Furthermore, when bithiophene-BODIPY donor–acceptor energy transfer probes are employed in these competition experiments, fluorescence and circular dichroism spectroscopy measurements in different regions of the visible spectrum additionally reveal intermolecular interactions occurring simultaneously at both sides of the macrocyclization reaction: the cyclic product, acting as a host for the competitor, and the monomer reactant, ultimately leading to macrocycle denaturation.

Introduction

Modern analytical chemistry offers a wide plethora of tools and techniques to study the structure and function of self-assembled systems and to measure diverse thermodynamic and kinetic parameters controlling their equilibria with other bound and unbound species.[1] However, as the system's complexity increases, the combination of multiple techniques that can provide complementary information on different concurrently competing equilibria is often required. Among them, fluorescence emission spectroscopy stands out as a very convenient technique that is non-invasive, provides high sensitivity and a short timescale, employs low analyte concentrations, and can be additionally implemented in microscopy and imaging. Fluorescence spectroscopy also allows for real-time monitoring of energy transfer events between photoexcited units. In this context, Förster resonance energy transfer (FRET) is a widely employed phenomenon in which the energy of a photoexcited donor fluorophore (d) is transferred to an energy-accepting unit (a) through long-range dipole–dipole interactions.[2] Such excitation transference depends on the relative orientation and distance between the donor and the acceptor, as well as on the spectral overlap of donor emission and acceptor absorption.

The study of FRET phenomena is thus considered as a potent tool to detect and monitor molecular interactions and dynamic changes.[3] The benefits of FRET have been exploited in polymer chemistry, as a method for the determination of polymer morphology,[3a,4] and in chemical biology, for the analysis of protein/DNA conformational changes[5] and for monitoring enzyme activity and intracellular molecular dynamics.[6] The area of supramolecular chemistry is also increasingly employing energy transfer events between donors and acceptors to unveil the

[a]*Nanostructured Molecular Systems and Materials Group, Departamento de Química Orgánica, Facultad de Ciencias, Universidad Autónoma de Madrid, 28049 Madrid, Spain. E-mail: maria.mayoral@uam.es; david.gonzalez.rodriguez@uam.es*

[b]*Institute for Advanced Research in Chemical Sciences (IAdChem), Universidad Autónoma de Madrid, 28049 Madrid, Spain*

† Electronic supplementary information (ESI) available: Synthetic details, compound characterization, DOSY experiments, emission and CD measurements and analysis of the titration and competition experiments. See DOI: 10.1039/c8sc03229g

thermodynamic and kinetic aspects of self-assembled synthetic systems. The groups of Rebek[7] and Diederich[8] were pioneers in the use of FRET to study the exchange kinetics and conformational switching events in supramolecular complexes. Supramolecular FRET probes have also been useful for investigating diverse characteristics of discrete self-assembled systems, such as isomer distribution of dimeric cyclic peptides;[9] guest inclusion in G-quadruplexes;[10] protein interactions with synthetic supramolecular elements;[11] or the dynamics in rotaxane,[12] foldaxane[13] and metal–ligand assemblies.[14] On the other hand, FRET phenomena are also helpful in polymeric noncovalent systems, for instance, to study the structure, thermodynamic stability, and cargo release mechanisms of vesicles and nanospheres;[15] to construct light-harvesting photosynthetic mimics;[10b,16] or to monitor monomer rearrangements or self-sorting events in supramolecular polymers.[17]

Here, we evaluate FRET processes as a tool to obtain thermodynamic information on noncovalent ring-chain equilibrium processes and, more concretely, on the case where the formation of ring assemblies is strongly favoured. When a molecule is endowed with (at least) two complementary binding sites, noncovalent association in solution may lead to competing equilibria between linear oligomers and cyclic assemblies (Fig. 1a).[18] A key parameter arises in the analysis of such systems: the effective molarity (EM), which affords an estimate of the propensity of the system to cyclize by comparing intra- and intermolecular association constants for a given binding event ($EM = K_{intra}/K_{inter}$), and therefore quantifies the chelate effect.[19] If the EM values are high and the overall concentration is maintained within certain limits, ring-chain equilibria may shift to the formation of a particular closed species, which is commonly the smallest, non-strained macrocycle. This is actually the basic principle used by supramolecular chemists to produce a wide variety of well-defined discrete architectures that often mimic those found in the natural world: helicates, ladders, grids, macrocycles, cubes, prisms, capsules, *etc.*

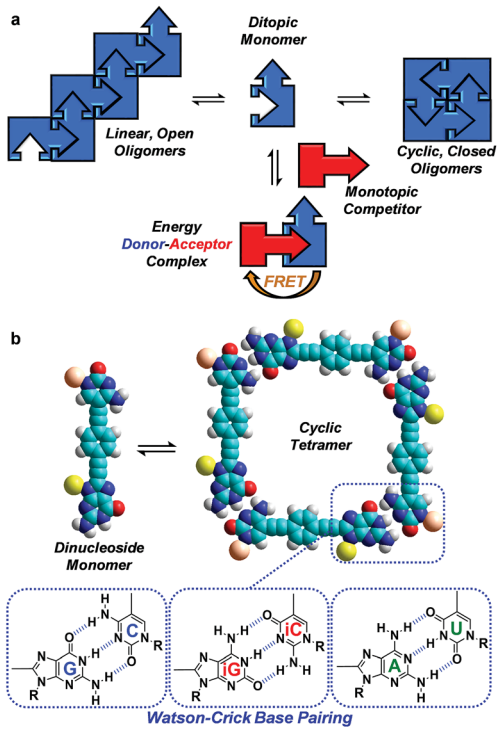

Fig. 1 (a) Scheme showing a competition between a ditopic FRET-donor molecule (in blue), able to establish an equilibrium between open linear oligomers and closed cyclic assemblies by complementary self-association, and a monotopic FRET-acceptor competitor (in red) equipped with the same binding motif. (b) Cyclic tetramer self-assembly through Watson–Crick G-C, iG-iC or A-U H-bonding interactions between dinucleoside monomers.

The determination of self-association equilibrium constants and the dissection of EM values from the overall free energy of the system are, however, not always simple practices. The approach we propose here is to set up a competition between a ditopic FRET-donor molecule, able to form closed cyclic assemblies by complementary self-association, and a monotopic FRET-acceptor competitor equipped with the same binding motif (Fig. 1a). Upon addition of increasing amounts of the competitor, the closed ensemble will progressively dissociate because this new species competes for the binding sites at the constituent molecules. Actually, in these experiments the intramolecular and intermolecular binding events are made to compete and constitute a very appropriate way to detach the intrinsic contribution of chelate cooperativity from the overall free energy of the system.

Our supramolecular case study involves dinucleoside monomers that self-assemble into H-bonded cyclic tetramers (Fig. 1b),[20] as recently demonstrated by us with molecules that comprised a *p*-diethynylbenzene central block substituted at the edges with the following lipophilic complementary nucleobases:[21] guanosine (G)-cytidine (C), 2-aminoadenosine (A)-uridine (U) or isoguanosine (iG)-isocytosine (iC).[22] The cyclotetramerization constants (K_T) were determined by diverse NMR and optical spectroscopy methods in different solvents and, from them, EMs were calculated and found to range between 10^2 and 10^3 M for the G-C (**GC**, Fig. 2) and iG-iC cyclic tetramers, a record value for this kind of cycle,[19e] and between 10^{-2} and 10^{-1} M for the A-U (**AU**, Fig. 2) macrocycle. This significant difference was ascribed to the unsymmetric nature of the ADD-DAA H-bonding pattern in the G-C and iG-iC monomers, as opposed to the symmetric ADA-DAD pattern of the A-U monomer, which largely contributes to the preorganization of the system toward cyclization.[21c]

In this work, with the aim of using FRET as an instrument to report intermolecular association, we designed and prepared a novel family of dinucleosides equipped with complementary G-C or A-U bases (**GdC**, **AdU**, **GaC** and **AaU**; Fig. 2). The ribose units were substituted with bulky lipophilic groups so as to increase solubility and prevent stacking interactions. As an energy donor (d), a benzo[1,2-*b*:4,5-*b*′]dithiophene unit, widely used in organic photovoltaics,[23] was employed. As an energy acceptor (a), a BODIPY[24] moiety was installed as a central block. This donor–acceptor pair displays absorption and emission maxima that are separated by about 200 nm and the donor emission partially overlaps with acceptor absorption in the 450–

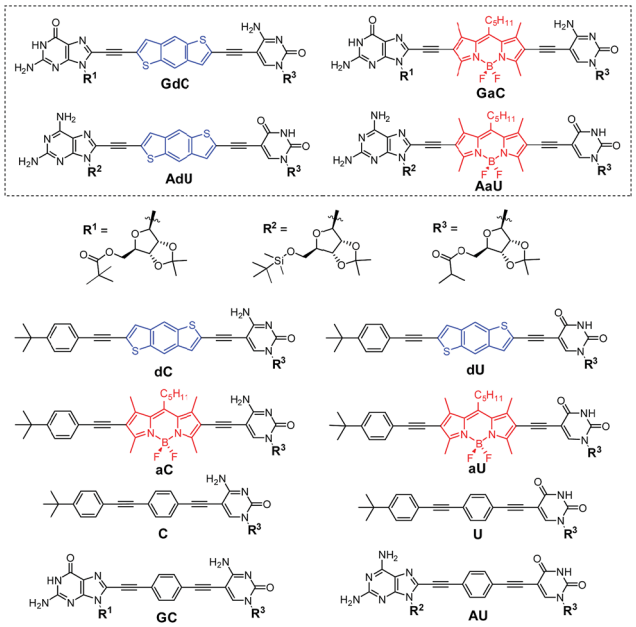

Fig. 2 Structure of mononucleosides C, U, dC, dU, aC and aU, dinucleosides GC and AU, and novel dye-labelled dinucleosides GdC, AdU, GaC and AaU.

550 nm region, which is a requirement for achieving high FRET efficiencies. Since optical spectroscopy measurements require low concentrations, an apolar aromatic solvent (toluene) was selected to maintain high association constants between nucleobases.[25] The most important photophysical parameters of these dye-conjugated molecules measured in toluene can be found in the ESI† accompanying this paper.

With this set of molecular probes, we demonstrate in this work that the combination of fluorescence spectroscopy and energy transfer phenomena, together with complementary tools such as circular dichroism (CD), can be a highly valuable strategy to extract supplementary thermodynamic information on complex supramolecular systems in which several equilibria participate concurrently. Here, the use of fluorescence spectroscopy not only allowed us to quantify chelate cooperativity, but also and for the first time, to discern and analyse simultaneously intermolecular interactions between FRET pairs occurring at the product (cyclic tetramer) and reactant (monomer) sides of a noncovalent reaction.

Results and discussion

Synthesis of dinucleoside monomers GdC, AdU, GaC and AaU

The dye-conjugated mononucleosides (**dC**, **dU**, **aC** and **aU**)[25] as well as the reference mono- (**C** and **U**)[26] and dinucleosides (**GC** and **AU**)[21a,c] shown in Fig. 2 have been previously described by us. Here, we report the synthesis and full characterization of novel donor (**GdC** and **AdU**) and acceptor (**GaC** and **AaU**) dinucleosides, which required two consecutive Pd-catalyzed couplings. In the first one, we connected 5-ethynylpyrimidine (**C1** and **U1**)[26] to the dibromobithiophene (**Br-*d*-Br**) or diiodoBODIPY (**I-a-I**) blocks and, subsequently, the corresponding 8-ethynylpurine (**G1** and **A1**)[26] was coupled (Scheme 1).

Analysis of the macrocyclization process. Determination of the degree of cyclotetramerization (χ_T)

Prior to performing the key competition experiments, we wanted to gain a clear insight into the initial situation, that is, the degree of self-association of our chromophore-dinucleoside monomers (**GdC**, **AdU**, **GaC** and **AaU**) into cyclic tetramers at different concentrations in toluene. In previous work we demonstrated by ^{1}H NMR experiments that **GC** (Fig. 2) displayed extremely high EMs, which resulted in strong *all-or-nothing* monomer-cycle equilibria. In contrast, EM values decreased dramatically for **AU** (Fig. 2), which resulted in a lower cyclic tetramer stability and, depending on the experimental conditions, the additional formation of small amounts of short open H-bonded oligomers (dimers, trimers,…).[21a,c] Unfortunately,

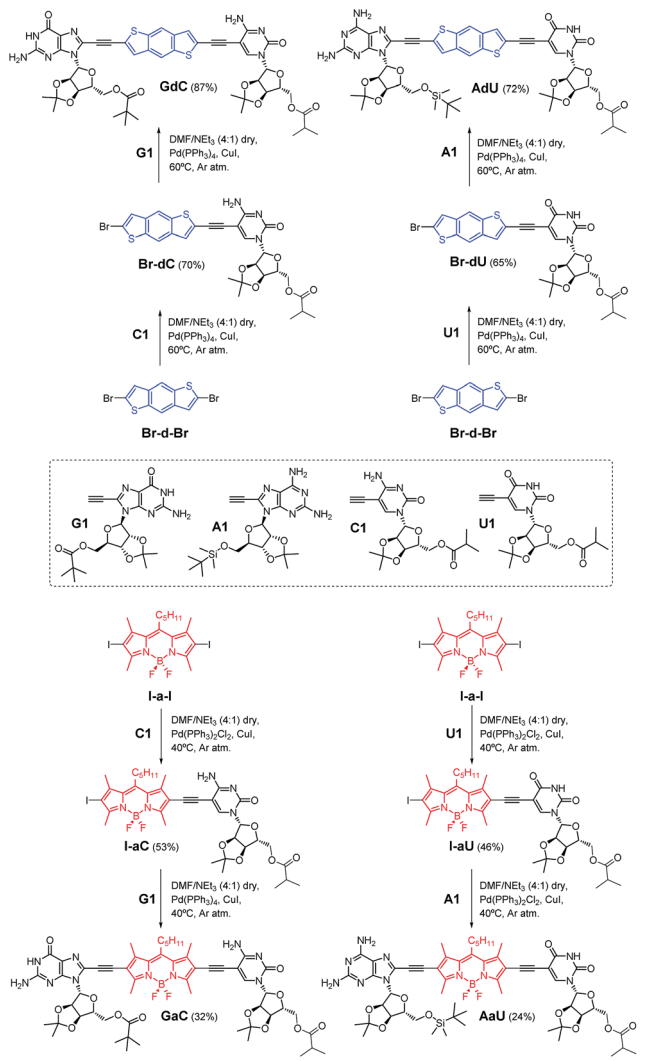

Scheme 1 Synthesis of dinucleosides GdC and AdU from dibromobithiophene Br-*d*-Br and GaC and AaU from diiodoBODIPY I-a-I *via* two consecutive Sonogashira coupling reactions.

^{1}H NMR analysis cannot be employed here because (1) the concentration range required is much higher than the one used in fluorescence spectroscopy, and (2) these compounds with large π-conjugated central blocks displayed poorly resolved ^{1}H signals in toluene-D_8 at such high concentrations.[27]

However, absorption and especially CD and emission spectroscopy experiments are also suitable tools to determine the degree of cyclotetramerization.[21] When the chiral monomers associate in cyclic species, fluorescence emission is appreciably quenched and red-shifted, and a Cotton CD effect arises. More concretely, **GdC** or **AdU** monomer emission exhibits two maxima below 460 nm (see, as representative examples, the red spectra in Fig. 3a and c), while the corresponding cyclic tetramers (***c*GdC$_4$** and ***c*AdU$_4$**) show a single maximum at around 530 nm (see, for instance, the blue spectra in Fig. 3a or 3c). For **GaC** and **AaU**, monomer and cyclic tetramer maxima in the BODIPY emission region show smaller but still measurable shifts (620 and 623 nm for **GaC** and 612 and 656 nm for **AaU**; see the red and blue spectra in Fig. 3d). On the other hand, the cyclic tetramers display Cotton effects at the bithiophene/BODIPY dye absorption maxima (negative for ***c*GdC$_4$** and positive for ***c*AdU$_4$**, ***c*GaC$_4$** and ***c*AaU$_4$**; see Fig. 3e–h) that vanish at high temperatures or low concentrations as a result of cyclic tetramer dissociation.[21]

These spectral changes in toluene can be monitored as a function of concentration (Fig. 3a–d) to evaluate quantitatively the molar fraction of molecules associated as cyclic tetramers (χ_T) in solution, and therefore the main equilibrium parameters associated with the macrocyclization process.[21a] We also performed temperature-dependent emission experiments at different concentrations within the 10^{-4} to 10^{-6} M range (Fig. S2A–D†) that support quantitatively the results obtained from the dilution measurements. Cyclic tetramer dissociation could be complementarily evaluated by monitoring the disappearance of the CD features with concentration and temperature (Fig. 3e–h). In all cases, an excellent correlation between CD and emission data was noted. In order to fit the experimental data, the following equilibria were considered that, in the case of the G-C couple, can be expressed as

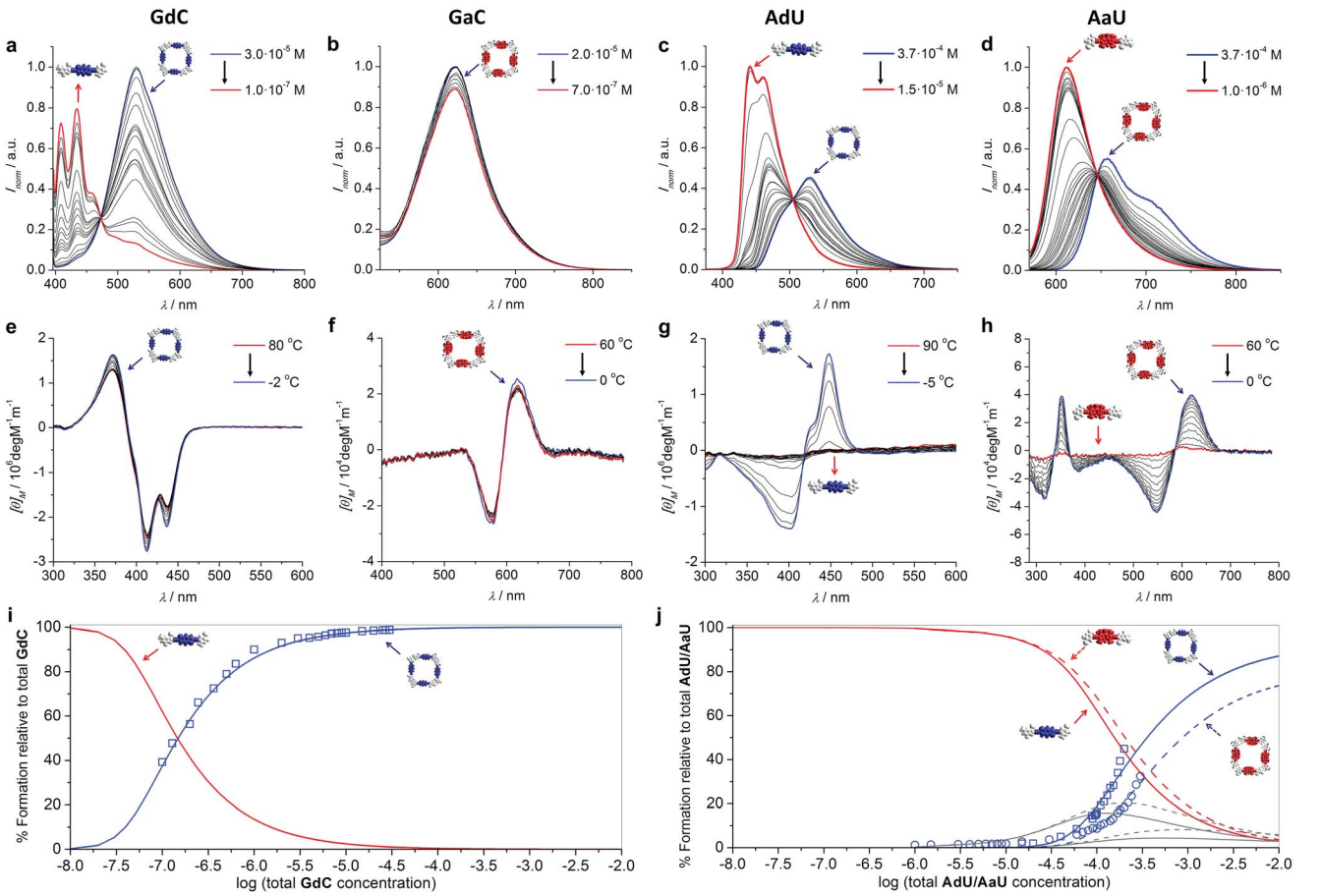

Fig. 3 (a–d) Concentration-dependent emission experiments ($T = 298$ K; toluene) of (a) **GdC** ($\lambda_{exc} = 385$ nm), (b) **GaC** ($\lambda_{exc} = 545$ nm), (c) **AdU** ($\lambda_{exc} = 365$ nm) and (d) **AaU** ($\lambda_{exc} = 555$ nm). (e–h) Temperature-dependent CD experiments of (e) **GdC** at 1.0×10^{-5} M, (f) **GaC** at 1.0×10^{-5} M, (g) **AdU** at 1.4×10^{-5} M and (h) **AaU** at 1.0×10^{-4} M in toluene. (i–j) Simulated speciation curves (lines) and experimental dilution data (squares for **GdC**/**AdU** and circles for **AaU**; calculated by using the areas within the measurement range) indicating the molar fraction of each species (cyclic tetramer: blue; monomer: red; open dimers and trimers: grey) as a function of the total concentration of (i) **GdC** and (j) **AdU** (solid lines)/**AaU** (dashed lines) in toluene. The dissociation of ***c*GaC$_4$** could not be analysed in the same way, but a comparison of (for instance) the CD spectra as a function of concentration/temperature (see Fig. 3e and f) suggests a similar stability to ***c*GdC$_4$**.

$$2\mathrm{GdC} \leftrightarrow \mathrm{GdC_2}\ (K = K_a) \quad (1)$$

$$3\mathrm{GdC} \leftrightarrow \mathrm{GdC_3}\ (K_2 = K_a^2) \quad (2)$$

$$4\mathrm{GdC} \leftrightarrow \mathrm{GdC_4}\ (K_3 = K_a^3) \quad (3)$$

$$4\mathrm{GdC} \leftrightarrow c\mathrm{GdC_4}\ (K_4\ \mathrm{EM} = K_a^4\ \mathrm{EM} = K_T) \quad (4)$$

$$5\mathrm{GdC} \leftrightarrow \mathrm{GdC_5}\ (K_4 = K_a^4) \quad (5)$$

$$6\mathrm{GdC} \leftrightarrow \mathrm{GdC_6}\ (K_5 = K_a^5) \quad (6)$$

where K is the equilibrium constant between Watson–Crick H-bonding pairs, and can be approximated using the reference association constant (K_a), previously determined from titration experiments in toluene with the corresponding mononucleoside combinations.[25] The only variable is hence K_T, which was calculated by multiwavelength analysis (see the ESI† for further details).[28] EM values for each dinucleoside cyclotetramerization process were then calculated using the relationship $\mathrm{EM} = K_T/K_a^4$. These thermodynamic parameters are displayed in the first three entries in Table 1 and show a good agreement with our previous work.[21c] They suggest that neither the presence of the rigid bithiophene/BODIPY unit as a central block instead of a *p*-phenylene group (compare **GC**/**AU** with **GdC**/**AdU** in Fig. 2) nor the change of the solvent medium to toluene has a profound influence on the chelate cooperativity of the system. Previously published work also supported the notion that EM values are typically not much impacted by the solvent nature,[29a,21a] unless specific solvation generates strain/steric effects between closely spaced binding sites, as determined recently.[29b]

Speciation curves, which reproduce the relative abundance of species as a function of overall concentration, were then simulated using the equilibrium parameters extracted from these dilution experiments.[30] In addition to monomer and cyclic tetramer species, short linear H-bonded oligomers (from dimers to hexamers; see eqn (1)–(6)) were included in these simulations. As shown in Fig. 3i and j, there exists a good correlation between simulated (solid lines) and experimental data (circles/squares) when representing the molar fraction of cyclic tetramers in solution.

All these results clearly indicate that the macrocycles formed by the G-C couple are far more robust than those associated with the A-U couple. For instance, under the conditions at which the competition experiments were carried out (298 K and 10^{-4} to 10^{-5} M range), ***c*GdC$_4$** and ***c*GaC$_4$** are associated almost quantitatively. As shown in Fig. 3i, S2A and S2B,† **GdC** and **GaC** fluorescence and CD spectra are virtually invariable under these conditions, and only start to display the typical monomer features at high temperatures and/or concentrations below 5×10^{-6} M. In sharp contrast, the molar fraction of **AdU** and **AaU** molecules associated as cyclic tetramers is just below 0.5 at the highest concentration measured, and decreases rapidly with temperature or concentration in the 5×10^{-4}–10^{-5} M concentration range (see Fig. 3j, S2C and S2D†). These results additionally confirm that the superior stability of the macrocycles assembled *via* G:C *versus* A:U base pair is not only due to the higher H-bonding strength of the G:C couple, but also due to the stronger chelate effect that this unsymmetric ADD-DAA binding interaction supplies when compared to the symmetric DAD-ADA pattern (see our previous work).[21c] The lower EM of **AdU** or **AaU** is reflected in the significant participation of small open oligomers, mainly dimers and trimers, in equilibrium at concentrations between 10^{-5} M and 10^{-2} M (see grey curves in Fig. 3j). **GdC**/**GaC**, in sharp contrast, display strong all-or-none features and cyclic tetramer and monomer species are seen as the only competing species in solution.

Table 1 Cyclotetramerization (K_T), peripheral binding (K_p) equilibrium constants and effective molarity (EM) calculated from the data obtained in different experiments in toluene

	K_a[c] [M^{-1}]	C[d] [M]	K_T [M^{-3}]	K_p [M^{-1}]	EM[e] [M]
GdC[a]	5.0×10^5		6.3×10^{24}		1.0×10^2
AdU[a]	2.0×10^3		3.2×10^{11}		2.0×10^{-2}
AaU[a]	2.0×10^3		1.0×10^{11}		6.3×10^{-3}
GdC + **aC**[b]	5.0×10^5	1.0×10^{-4}	—[f]	—[f]	—[f]
		2.0×10^{-5}	8.9×10^{24}	1.4×10^4	1.4×10^2
		1.0×10^{-5}	8.3×10^{24}	1.1×10^4	1.3×10^2
		5.0×10^{-6}	2.5×10^{25}	1.7×10^4	4.0×10^2
		Dilution[g]	6.3×10^{24}	8.5×10^4	1.0×10^2
AdU + **aU**[b]	2.0×10^3	1.1×10^{-4}	3.5×10^{11}	1.0×10^3	2.2×10^{-2}

[a] Data obtained from concentration-dependent experiments (Fig. 3). [b] Data obtained from competition experiments (Fig. 5). [c] Reference association constant between complementary nucleosides in toluene.[25] [d] Dinucleoside (**GdC** or **AdU**) concentration used in the competition experiment. [e] Effective molarities were calculated as EM = K_T/K_a^4. [f] Not fitted. [g] Fitting of the dilution experiment at a constant [**GdC**]/[**aC**] 1 : 1 ratio (see Fig. 8).

Analysis of the macrocyclization process by competition experiments with complementary mononucleosides

Once we gained a clear insight into the self-assembly of our dinucleoside molecules in toluene solutions, we set up competition experiments between the ditopic donor molecule (**GdC** or **AdU**) and a monotopic pyrimidine acceptor that does not bear the energy-accepting functionality (**C** or **U**, respectively; see Fig. 2), and that will compete for binding to the purines (see Fig. 4a for a schematic representation). In order to start from a situation where the maximum number of molecules are associated as cyclic species, the total donor dinucleoside concentration in toluene was kept constant throughout the titration experiment above 10^{-5} M for **GdC** and just over 10^{-4} M for **AdU**. According to the previous results, these concentrations afford cyclic tetramer molar fractions of $\chi_T \sim 1.0$ for **GdC**, which is the ideal situation, and $\chi_T \sim 0.25$ for **AdU**. Fluorescence spectroscopy can be used here due to the different emission features of the dinucleoside monomers as a function of the association state: either as a cyclic tetramer at the beginning of the titration, or as a bimolecular **GdC**·**C**/**AdU**·**U** complex at the end of the titration (see Fig. 4a). The excitation wavelength was set at 385 nm, a region where the reference **C** or **U** mononucleosides do not absorb, so only the **GdC**/**AdU** dinucleoside chromophores are excited. Fig. 4b and c show, as an example, the evolution of the fluorescence spectrum of **GdC**/**AdU** upon gradual addition of **C**/**U**, respectively.

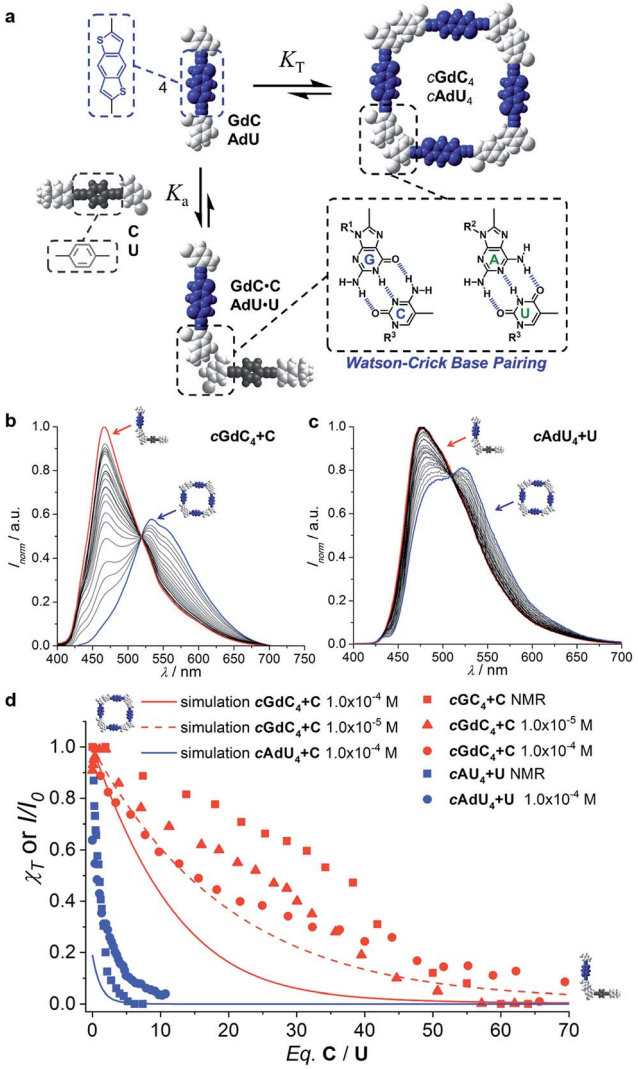

Fig. 4 (a) Schematic representation of the competition experiment between GdC/AdU dinucleosides and C/U mononucleosides. Cyclic tetramers are in equilibrium with monomers (K_T) and, under the conditions at which the competition experiments were carried out, such equilibrium is strongly (GdC) or moderately (AdU) shifted to the macrocycle side. Upon addition of the complementary C/U mononucleoside, a competing equilibrium is established in which the free dinucleoside monomer binds to the mononucleoside stopper (K_a), which shifts the cyclotetramerization equilibrium toward the formation of GdC·C/AdU·U pairs. (b and c) Normalized fluorescence emission changes (λ_{exc} = 385 nm, T = 298 K, toluene) observed in the titration of (b) GdC with increasing amounts of C ([GdC] = 1.0 × 10^{-4} M, [C] = 1.4 × 10^{-2} M) and (c) AdU with increasing amounts of U ([AdU] = 1.4 × 10^{-4} M, [U] = 3.0 × 10^{-3} M). (d) Representation of the degree of cyclic tetramer association (χ_T) or emission changes (I/I_0) as a function of the equivalents of complementary pyrimidine mononucleoside added for GdC + C ([GdC] = 1.0 × 10^{-4} M (red circles) or 1.0 × 10^{-5} M (red squares; see Fig. S3A†)) and for AdU + U ([AdU] = 1.4 × 10^{-4} M (blue circles)). For the sake of comparison, we also include previous results obtained in competition experiments between GC/AU and C/U measured by ^{1}H NMR at 10^{-2} M concentration in $CDCl_3$ (red and blue squares).[21c] Speciation curves were simulated using the previously calculated K_a and K_T values (Table 1).

The changes observed resemble those obtained in concentration- or temperature-dependent experiments (see Fig. 3a–d and S2†): as the cyclic tetramer dissociates, a blue-shift in emission maxima and a moderate intensity enhancement are noted. However, the final spectra (in red) obtained in these titrations, with maxima at 464 nm for **GdC** + **C** and 477 for **AdU** + **U** are not exactly the same as in the dilution measurements, since the final species (*i.e.* the **GdC·C**/**AdU·U** complex or **GdC**/**AdU** dinucleoside, respectively) is also different (please compare Fig. 4b and c with Fig. 3a and c).

While the emission changes in the course of these titrations are similar for **GdC** and **AdU**, the number of equivalents of complementary pyrimidine mononucleoside required to reach saturation is very different for each base pair (please compare the red and blue solid circles in Fig. 4d). Whereas more than *ca.* 60 equivalents of **C** are required to denature the cyclic ***c*GdC$_4$** assemblies, less than *ca.* 10 equivalents of **U** are needed to fully dissociate ***c*AdU$_4$**. The trends recorded also show a reasonable match with those obtained through previously reported competition experiments with dinucleosides **GC** and **AU** (also included in Fig. 4d for comparison),[21c] despite the fact that different molecules (**GdC**/**AdU** *vs.* **GC**/**AU**), solvents (toluene *vs.* $CDCl_3$), concentration ranges (10^{-2}–10^{-3} M *vs.* 10^{-4}–10^{-5} M), techniques (emission *vs.* ^{1}H NMR spectroscopy) and physical observables were employed.

Using the previously calculated K_a and K_T values (Table 1), we built speciation curves and compared them with the molar fraction of molecules associated as cyclic tetramers (χ_T) obtained at each titration point for all **GdC** + **C** (at 10^{-4} and 10^{-5} M; see Fig. S3A†) and **AdU** + **U** (at 10^{-4} M) competition experiments. An additional equilibrium was considered that, in the case of the G-C couple, can be expressed as

$$\mathrm{GdC} + \mathrm{C} \leftrightarrow \mathrm{GdC{\cdot}C}\ (K' = K_a) \qquad (7)$$

where, again, we made the approximation that Watson–Crick binding in the **GdC·C**/**AdU·U** species (K') is equal to the one calculated for the corresponding mononucleoside mixtures in toluene (K_a; see Table 1).[25] As can be noted in Fig. 4d, the simulations show only a modest agreement with the experimental results for **AdU** + **U** at 10^{-4} M (blue curve) and for **GdC** + **C** at 10^{-5} M (red dashed curve), but they deviate substantially from the trends obtained for **GdC** + **C** at 10^{-4} M (red solid curve). As a matter of fact, the overall competition equilibrium we are considering

$$\textbf{\textit{c}GdC}_4 + 4\mathrm{C} \leftrightarrow 4\mathrm{GdC{\cdot}C}\ (K_C)$$

should be concentration-dependent, since the number of species at the product side is lower than that at the reagent side, and should shift to the formation of **GdC·C** at higher concentrations. This means that, for a given set of K_a and K_T values, the denaturation trends obtained in these competition titrations should decay more abruptly as the concentration is increased, just as the simulations show (see also Fig. S3B,† where we simulate denaturation at different concentrations within the 10^{-2}–10^{-6} M range). In contrast, our experiments revealed quite

similar denaturation curves for the titration of **GdC** with **C** at both concentrations. However, as we found out in the next set of experiments (see below), in these competition experiments we do not consider a relevant additional equilibrium taking place in solution between **GdC**/**AdU** dinucleosides and **C**/**U** mononucleosides.

Analysis of the macrocyclization process by competition experiments with FRET-dye-labelled complementary mononucleosides

One of the aims of this work is to address and report supramolecular interactions by utilizing energy transfer processes with FRET couples. Thus, we carried out the same kind of denaturation experiments of ***c*GdC$_4$** and ***c*AdU$_4$** now in the presence of increasing amounts of the corresponding mononucleosides bearing the complementary energy-acceptor dye **aC** or **aU** (see Fig. 5a).

An example of the fluorescence spectral changes recorded in these titrations with **GdC** and **AdU** is shown in Fig. 5b and c, respectively. In order to maximize the FRET effect, the excitation wavelength was set at 385 nm, where the donor/acceptor absorption ratio reaches a maximum. As expected, donor emission is gradually quenched as increasing amounts of **aC** or **aU** are added. This is supposedly due to the formation of the corresponding donor–acceptor complex (**GdC**·**aC** and **AdU**·**aU**, as shown in Fig. 5a), in which the donor bithiophene emission is strongly quenched by energy transfer to the BODIPY acceptor. At the same time, acceptor emission is enhanced in the course of the titrations, which is partly due to the energy transfer event, but mainly due to the fact that the concentration of acceptor molecules is increased constantly in the experiment.

The fluorescence intensity within the donor emission range (450–560 nm) was then plotted as a function of the equivalents of mononucleoside acceptor added (Fig. 5d; red and blue open circles). It is clearly evident that donor emission, either **GdC** or **AdU**, is virtually fully quenched (>95%) after the addition of a few equivalents (*i.e.* <4 eq.) of complementary acceptor. These results strongly contrast with the trends previously obtained for ***c*AdU$_4$** and ***c*GdC$_4$** denaturation, respectively, using the changes in emission maxima (see Fig. 4), which are also reproduced in Fig. 5d for the sake of comparison (red and blue closed circles).

We believe that the most reasonable explanation for such a significant deviation comes from the fact that we must now take into account other competing equilibria, as is shown schematically in Fig. 5a: the binding of the mononucleoside acceptor (**aC** or **aU**) to external sites at the cyclic tetramer periphery, without actually causing macrocycle dissociation. Such peripherally bound ***c*GdC$_4$**·**aC**/***c*AdU$_4$**·**aU** species also combines FRET donor and acceptor molecules, and therefore its formation should contribute as well to the gradual **GdC**/**AdU** emission quenching observed. The participation of this species should be mostly manifested at the beginning of the titrations, where only a few equivalents of acceptor quencher are added, and for the stronger ***c*GdC$_4$** assembly, which can withstand a higher amount of mononucleoside competitor. A tentative association mode for ***c*GdC$_4$**·**aC**, where the C pyrimidine forms

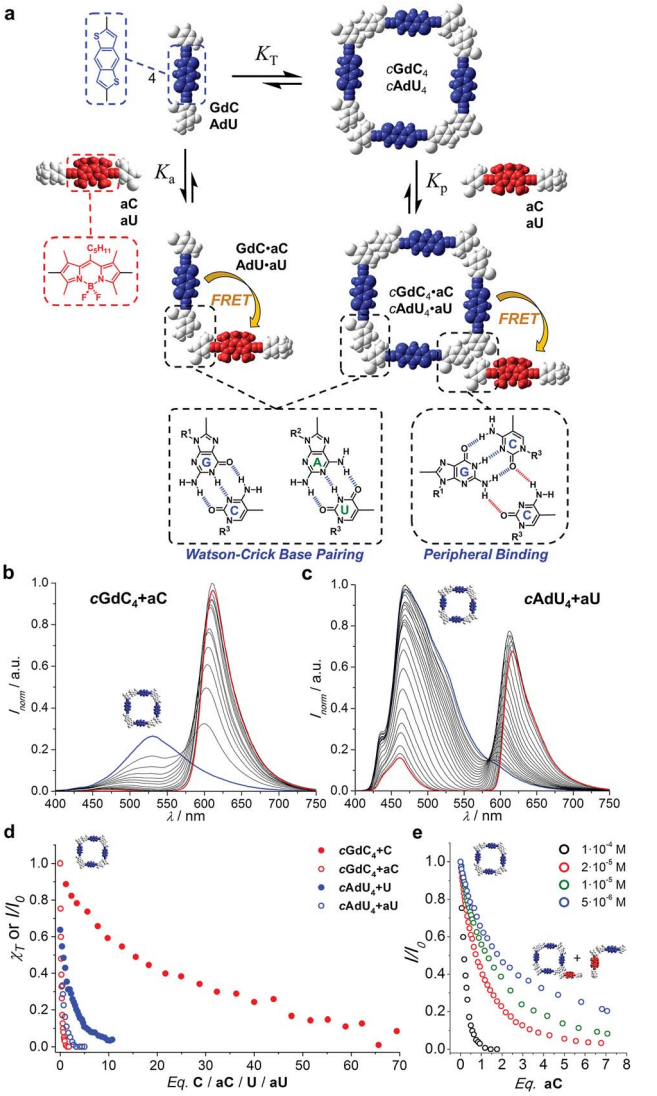

Fig. 5 (a) Schematic representation of the competition experiment between **GdC**/**AdU** dinucleosides and **aC**/**aU** mononucleosides. Cyclic tetramers are in equilibrium with monomers (K_T) and, under the conditions at which the competition experiments were carried out, such equilibrium is strongly (**GdC**) or moderately (**AdU**) shifted to the tetramer side. Upon addition of the complementary mononucleoside, two competing equilibria, both of them resulting in donor emission quenching due to energy transfer, would be established: (1) peripheral binding (K_p) to external sites of the cyclic tetramer (a hypothetical binding mode of **aC** to ***c*GdC$_4$** is shown) and (2) binding to the free dinucleoside monomer (K_a), which will shift the cyclotetramerization equilibrium toward the formation of **GdC**·**aC**/**AdU**·**aU** FRET pairs. (b and c) Normalized fluorescence emission changes (I/I_0; $\lambda_{exc} = 385$ nm, $T = 298$ K, toluene) observed in the titration of (b) **GdC** with increasing amounts of **aC** ([**GdC**] = 1.0 × 10^{-4} M, [**aC**] = 2.0 × 10^{-4} M) and (c) **AdU** with increasing amounts of **aU** ([**AdU**] = 1.1 × 10^{-4} M, [**aU**] = 4.7 × 10^{-4} M). (d) Representation of the degree of cyclic tetramer association (χ_T) or emission changes (I/I_0), as a function of the equivalents of complementary pyrimidine mononucleoside added for **GdC** + **C** (Fig. 4b; [**GdC**] = 1.0 × 10^{-4} M; red solid circles), **AdU** + **U** (Fig. 4c; [**AdU**] = 1.4 × 10^{-4} M; blue solid circles), **GdC** + **aC** (Fig. 5b; [**GdC**] = 1.0 × 10^{-4} M; red open circles), and **AdU** + **aU** (Fig. 5c; [**AdU**] = 1.1 × 10^{-4} M; blue open circles). (e) Normalized emission changes of **GdC** as a function of the equivalents of **aC** added at different **GdC** concentrations (see also Fig. S3C†).

two H-bonds with the G-amine proton and the C-carbonyl lone pair that are not participating in Watson–Crick interactions, is shown in Fig. 5a. Other binding modes or binding of more than one energy-accepting unit to the cyclic tetramers are, of course, also plausible, but cannot be assessed through the spectroscopic techniques employed in this work.

In order to corroborate the presence of this additional equilibrium and prove the formation of ***c*GdC$_4$·aC** and ***c*AdU$_4$·aU** species, where the competitor binds to non-dissociated macrocycles, we performed different sets of complementary experiments.

First, we reasoned that the formation of the ***c*GdC$_4$·aC** assemblies should be favoured at higher concentrations. Therefore, supplementary competition experiments were carried out at different initial **GdC** concentrations: 1.0×10^{-4}, 2.0×10^{-5}, 1.0×10^{-5} and 5.0×10^{-6} M (see Fig. S3C†). As can be observed in Fig. 5e, at the beginning of the titrations, when only a few equivalents of **aC** are added, the original **GdC** fluorescence is quenched to a higher extent at higher concentrations. In other words, the relative amount of **aC** required to achieve a given quenching factor is lower as the overall concentration increases. This trend supports the hypothesis of an associative process where **aC** would bind to ***c*GdC$_4$** and activate energy transfer between bithiophene and BODIPY units.

On the other hand, despite the strong quenching and very low **GdC** residual emission, it is interesting to note that the characteristic blue emission shift from *ca.* 530 to 460 nm (as noted in the transformation of ***c*GdC$_4$** to **GdC·C**; Fig. 4b) was also detected in the course of the titrations of ***c*GdC$_4$** with up to 100 equivalents of **aC** (see Fig. S3D†). This observation confirms that the **GdC·aC**/**AdU·aU** species, resulting from cyclic tetramer dissociation at high **aC**/**aU** relative concentrations, are still the main products at the end of these titrations.

Additionally, monitoring these competition experiments by CD spectroscopy proved to be a helpful source of complementary information that confirmed that the cyclic tetramers are not dissociated at the beginning of the titrations with **aC**, despite the strong quenching recorded. The bithiophene and BODIPY dinucleosides, besides being complementary FRET pairs, absorb in different regions of the visible spectrum. Thus, swapping the energy donor and acceptor functionalities in the dinucleoside and mononucleoside molecules (that is, using **GaC** + **dC** and **AaU** + **dU** combinations) allowed us to isolate and record the CD spectra of the ***c*GaC$_4$** and ***c*AaU$_4$** cyclic tetramers (between 500 and 700 nm) without contamination due to the strong absorption of the excess of **dC**/**dU** competitor (at *ca.* 400 nm) (Fig. 6a).[31] The opposite combination, that is, ***c*GdC$_4$** + **aC** or ***c*AdU$_4$** + **aU**, used in the fluorescence quenching experiments, was also tested with similar results, but suffers from absorption saturation from the excess of **aC**/**aU** molecules in the **GdC**/**adU** absorption region, which produces a considerable distortion of the CD spectra, as shown as an example in Fig. S3E.† Therefore, another type of competition experiment was performed in which cyclic tetramer denaturation in the presence of increasing amounts of **dC**/**dU** was monitored by the disappearance of the characteristic ***c*GaC$_4$**/***c*AaU$_4$** CD signals at

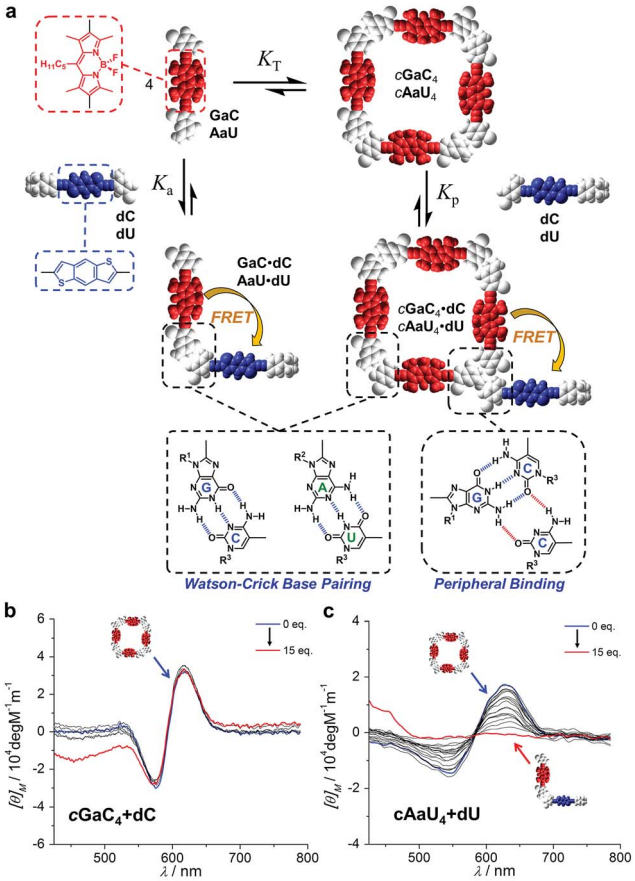

Fig. 6 (a) Schematic representation of the competition experiment between GaC/AaU dinucleosides and dC/dU mononucleosides (see also Fig. 4). CD signal changes (λ_{exc} = 385 nm, T = 298 K, toluene) observed in the titration of (b) GaC with increasing amounts of dC ([GaC] = 1.0×10^{-4} M, [dC] = 7.0×10^{-3} M) and (c) AaU with increasing amounts of dU ([AaU] = 1.0×10^{-4} M, [dU] = 2.8×10^{-3} M).

around 600 nm. The results are shown in Fig. 6b and c, respectively.

It is evident that the addition of **dC** does not produce major changes in the CD spectrum of ***c*GaC$_4$**, indicating that, at least up to 15 equivalents of competitor, this cyclic species does not suffer from significant denaturation at 1.0×10^{-4} M (see also Fig. S3F,† in which the same experiment was performed at a concentration one order of magnitude lower). Further addition, up to 72 eq. of **dC**, led to the disappearance of this CD signal, but it could not be properly monitored because the huge excess of donor began to interfere in this absorption region as well. In sharp contrast, the characteristic ***c*AaU$_4$** CD signal is gradually lost with the addition of up to *ca.* 10 eq. of **dU**. These results are in good agreement with the trends shown in Fig. 4d and substantiate the idea that, due to the large differences in EM, the ***c*GdC$_4$**/***c*GaC$_4$** and ***c*AdU$_4$**/***c*AaU$_4$** cyclic systems are insignificantly and totally dissociated, respectively, upon addition of a small excess of the complementary mononucleoside. These CD titrations also verify the hypothesis that the strong **GdC** emission quenching observed after the addition of the first **aC** equivalents (Fig. 5b) is caused by the interaction between

***c*GdC$_4$** and **aC** in a way that must be different to ring-opening *via* Watson–Crick competition.

Analysis of the peripheral association between mononucleosides and dinucleoside macrocycles

In short, it is evident that the use of FRET pairs, where energy donors and acceptors communicate with each other, has the advantage of reporting additional binding events occurring in solution, namely the interactions between non-dissociated cyclic tetramers and mononucleoside molecules, which is especially clear in the case of **GdC** when compared to **AdU**. Therefore, in order to fit the **GdC**/**AdU** donor emission deactivation trends in the presence of **aC**/**aU**, a supplementary process (see also Fig. 5a) was now considered in addition to equilibria (1)–(7) that takes into account peripheral binding, which, for the G-C couple, can be expressed as

$$c\mathrm{GdC_4} + \mathrm{aC} \leftrightarrow c\mathrm{GdC_4}\cdot\mathrm{aC}\ (K_\mathrm{p}) \quad (8)$$

Both K_T and K_p were calculated simultaneously and the results are shown in Table 1 (see Fig. S3G and S3H† for further details). The term K_p should be regarded as an apparent association constant that describes the binding of quencher molecules to the macrocycle, resulting in donor emission deactivation, and was calculated to be $K_\mathrm{p} = 10^4$–10^5 M^{-1} for ***c*GdC$_4$·aC** and $K_\mathrm{p} = 10^3$ M^{-1} for ***c*AdU$_4$·aU** in toluene. Unfortunately, from all the data collected we cannot determine the number of quencher molecules that can bind to the cyclic tetramers, or if subsequent binding events quench donor fluorescence in the macrocycle to the same extent as the first one.

This model comprising multiple competing equilibria provides an insight into the relative population of the different supramolecular species during the titrations. New speciation curves[30] were simulated including the peripheral binding equilibrium (8) and they are now able to reproduce rather satisfactorily both the donor emission quenching behaviour observed for our ***c*GdC$_4$**/***c*AdU$_4$** macrocycles in the course of the titration experiments with **aC**/**aU** (Fig. 5) and the emission changes recorded in the titrations with **C**/**U** (Fig. 4).

Fig. 7a thus provides an accurate picture of the distribution of species that coexist at different [**aC**] (or [**C**])/[**GdC**] ratios. At low [**aC**]/[**GdC**] ratios, the ***c*GdC$_4$·aC** assembly is formed in significant amounts (green curve), but its concentration then decreases at higher **aC** equivalents in favour of the bimolecular **GdC·aC** complex (red curve). Both of these complexes, where energy donors and acceptors are non-covalently bound, contribute to the emission quenching observed for the **GdC** molecule (open blue circles; see Fig. 5), which fits quite well with the disappearance of ***c*GdC$_4$** to yield ***c*GdC$_4$·aC** and **GdC·aC** (blue line).

Furthermore, the introduction of equilibrium (8) in the simulations leads to comparable K_T and K_p values when employing different **GdC** concentrations, and reproduces the concentration-dependent behaviour observed in the ***c*GdC$_4$** fluorescence deactivation trends in the presence of **aC** (Fig. 5e). The relative abundance of this cyclic species (blue curves in Fig. 7b) is seen to decrease more abruptly at higher

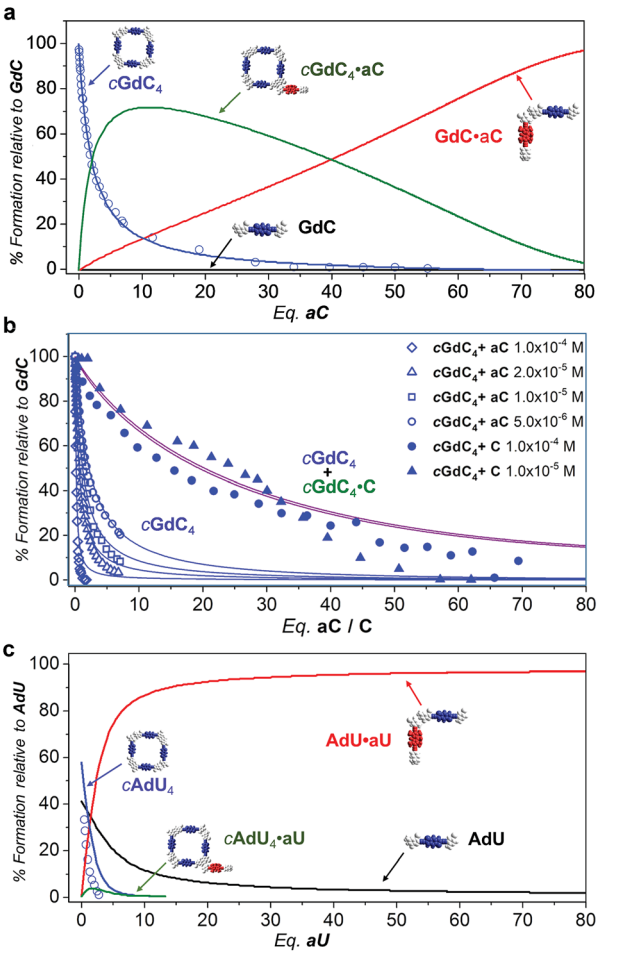

Fig. 7 Simulated speciation profiles (lines; using the K_a, EM and K_p values displayed in Table 1) and experimental titration data obtained from the donor emission quenching trends (open shapes; see Fig. 5) or emission shifts (solid shapes; see Fig. 4) for the competition experiments of (a and b) ***c*GdC$_4$** + **aC** (or **C**) at (a) a single (b) or different concentrations (see Fig. 4d and 5e), or (c) ***c*AdU$_4$** + **aU** (or **U**) in toluene.

concentrations, which is mostly due to an equilibrium shift toward the formation of peripherally bound ***c*GdC$_4$·aC**.

However, the peripherally bound ***c*GdC$_4$·C** species cannot be detected without the assistance of FRET events. Even if it is presumably being formed in the course of the titration experiments with **C**, monitored by changes in the emission spectra (Fig. 4), it must exhibit very similar emission (and CD) features to ***c*GdC$_4$**. Nonetheless, its formation does affect the overall equilibrium by sequestering **C** competitor molecules, so equilibrium (8) should be additionally taken into account when simulating the cyclic tetramer denaturation curves shown in Fig. 4d. Therefore, in this case the combined ***c*GdC$_4$** and ***c*GdC$_4$·C** relative abundances must be considered, which results in the purple curves in Fig. 7b. These "addition" curves now reproduce reasonably well the changes observed in the emission spectra as the number of **C** competitor equivalents increases (Fig. 4). Moreover, the combined model predicts a very weak dependence on the total concentration, which suggests that the presence of equilibrium (8) introduces a "buffering"

effect by diminishing the relative amount of competitor molecules available for the denaturation equilibrium. This is in line with our experimental observation that cyclic tetramer denaturation, monitored with different techniques at different concentrations (as shown in Fig. 4d), is not extraordinarily sensitive to the overall concentration (please also see Fig. S3B†).

Similarly, Fig. 7c describes the picture obtained in the simulations of the competition titrations of **AdU** with **U** or **aU**. This system is far less interesting in the context of the results described in this work, since the binding constant between complementary nucleobases and the EM values are significantly lower. This makes the ***c*AdU$_4$** macrocycle much weaker, and its formation was far from quantitative under the initial conditions of our competition experiments. Moreover, as a consequence of a much lower chelate cooperativity, ***c*AdU$_4$** (blue curve) dissociates abruptly at low [**U**]/[**AdU**] ratios to yield the **AdU·U** species (red curve) in equilibrium with the **AdU** monomer (black curve), and the participation of peripherally bound ***c*AdU$_4$·U** species (green curve) becomes insignificant and cannot be properly monitored.

Finally, in view of the results obtained, we were intrigued to examine the effect of changing the overall concentration on the different competition equilibria between **GdC** and **C** or **aC** at constant [**C**] (or [**aC**])/[**GdC**] ratios. For such a goal, we performed dilution experiments (Fig. 8) monitored by emission (in the 1.0×10^{-4}–3.3×10^{-8} M range) and CD spectroscopy (in the 1.0×10^{-4}–5.2×10^{-6} M range) of three different samples: (1) **GdC**, (2) **GdC** with 10 equivalents of **C**, and (3) **GdC** with 1 equivalent of **aC**.

As already shown in Fig. 3, within this concentration range the ***c*GdC$_4$** macrocycle is not significantly dissociated in toluene and the normalized **GdC** emission, with a maximum at 530 nm, and CD spectra remain virtually unaltered (see Fig. 8a and b). Only at the lowest concentrations, which could only be studied by fluorescence spectroscopy, do the monomer emission bands start to rise below 450 nm.

We then compared these results with the dilution of **GdC** in the presence of the competitor. In the case of the 1 : 10 **GdC** + **C** mixture (Fig. 8c and d), no significant changes were noted within the 10^{-4}–5×10^{-6} M range. According to our model, the most abundant species under these conditions should be ***c*GdC$_4$·C**, in equilibrium with small amounts of **GdC·C**. The emission maxima found at 525 nm can be attributed to the first cyclic species (please compare them with the emission maxima of the pristine ***c*GdC$_4$** macrocycle in Fig. 8a), while the smaller bands at 470 and 435 nm seem to indicate the presence of the latter non-cyclic species. If the concentration is reduced to 10^{-8} M, the typical **GdC** monomer emission bands below 450 nm progressively become more abundant. Likewise, the CD spectra recorded between 10^{-4} and 5×10^{-6} M are similar to those recorded for ***c*GdC$_4$**, confirming the presence of cyclic species, though it is slightly perturbed by the presence of a large excess of **C**, especially at high concentrations.

Finally, for the 1 : 1 **GdC** + **aC** combination (Fig. 8e and f), the emission spectra revealed a considerably quenched **GdC** emission at high concentrations, as expected in view of the previous results. However, as the concentration decreases at a constant

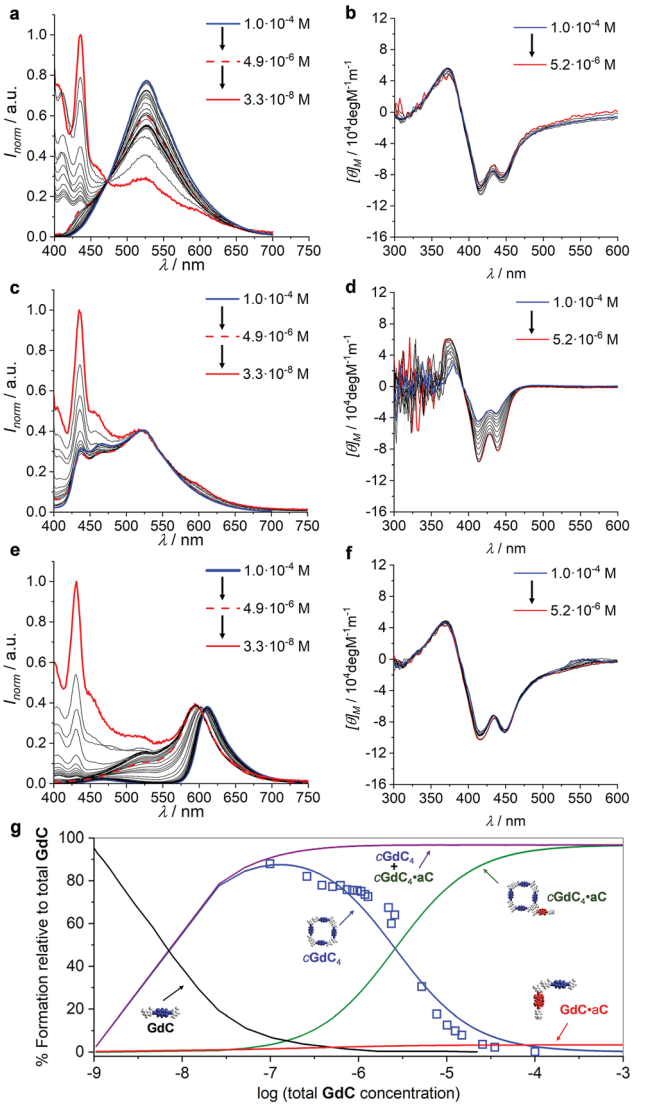

Fig. 8 (a, c, and e) Normalized emission spectra at different concentrations within the 1.0×10^{-4}–3.3×10^{-8} M range and (b, d, and f) CD spectra at different concentrations within the 1.0×10^{-4}–5.2×10^{-6} M range of (a and b) **GdC**, (c and d) a 1 : 10 **GdC** + **C** mixture or (e and f) a 1 : 1 **GdC** + **aC** mixture. (g) Speciation profiles (lines; simulated using the values shown in Table 1) and calculated E_{FRET} values at different concentrations (blue open squares) within the 10^{-2}–10^{-9} M range.

GdC : aC 1 : 1 ratio, the ***c*GdC$_4$** emission features, with a maximum at 530 nm, are gradually recovered, which is in agreement with the dissociation of the peripherally bound ***c*GdC$_4$·aC** complex and in line with the titrations at different concentrations shown in Fig. 5e. The degree of emission quenching (or FRET efficiency) was then calculated as $E_{FRET} = 1 - (I_{DA}/I_D)$, where I_D and I_{DA} are the fluorescence emission intensities under the same experimental conditions of the donor molecule in the absence (Fig. 8a) or presence (Fig. 8e) of the corresponding acceptor, respectively, at the 530 nm emission maximum, where the **aC** molecule does not emit. The calculated E_{FRET} can be related to the molar fraction of emitting **GdC** molecules, which are mostly associated as cyclic tetramers

above 5×10^{-6} M, and is represented in Fig. 8g as open blue squares. Again, the CD spectra recorded in this concentration range do not change and exhibit comparable intensity to the one obtained for **GdC** alone (compare Fig. 8b and f), thus confirming the persistence of cyclic species, either ***c*GdC$_4$** or ***c*GdC$_4$·aC**.

The quantitative analysis of these dilution experiments, using again the previously calculated K_a, EM and K_p values (Table 1), provided an accurate picture of the relative distribution of species as a function of concentration, which is represented in Fig. 8g for the **GdC : aC** 1 : 1 mixture within the 10^{-2}–10^{-9} M range. The ***c*GdC$_4$·aC** species dominate at high concentrations, competing with a small amount of **GdC·aC**. As shown in Fig. S4,† where similar speciation profiles were generated by changing K_a, EM and K_p values, the degree of participation of the bimolecular **GdC·aC** species depends on the magnitude of EM and K_p, but not on K_a. Both species are responsible for the quantitative **GdC** emission quenching observed under these conditions. Dilution down to 5×10^{-6} M leads primarily to the dissociation of **aC** from the macrocycle periphery and to the gradual release of emissive ***c*GdC$_4$** cyclic tetramers. It is important to note that the evolution of ***c*GdC$_4$** is in reasonable agreement with the calculated E_{FRET} values at each concentration point. Therefore, within this 10^{-2}–10^{-6} M range peripherally bound ***c*GdC$_4$·aC** and unbound ***c*GdC$_4$** macrocycles are the main species in solution, and the equilibrium between them depends exclusively on K_p, but not on EM or K_a (see Fig. S4†). Interestingly, the sum of the relative abundances of these two cyclic species (purple curve in Fig. 8g) is almost constant within this concentration window, which is in agreement with the trends observed in Fig. 8c, where the shape of the emission spectra did not display important changes down to 10^{-6} M. Hence, these dilution experiments supported the notion that, if peripheral binding comes into play, a "buffering" effect is introduced and the overall equilibrium in the presence of a competitor is not strongly dependent on concentration. Finally, decreasing the concentration below 10^{-6} M produces the dissociation of both cyclic and non-cyclic species, and the **GdC** monomer, characterized in the emission experiments by two maxima at 435 and 415 nm, dominates in the low concentration regime. As shown in Fig. S4,† the concentration at which this species comes into play depends on K_a and EM, but not on K_p.

Conclusions

This whole analysis led us to conclude that the measurement of FRET phenomena, which basically report the proximity of donor and acceptor pairs and therefore the presence of specific binding interactions, can be very useful to obtain supplementary information from a supramolecular association landscape that other techniques, such as NMR or absorption/CD spectroscopy, fail to disclose. In particular, a noncovalent macrocyclization process has been studied here by means of fluorescence emission spectroscopy by setting up a competition between a ditopic monomer, which bears complementary purine–pyrimidine bases at the edges and self-associates in cyclic tetramers in solution, and a monotopic pyrimidine molecule that is gradually added to the solution and that will compete for binding to the purine units. Multiwavelength fitting of the emission changes experienced by the monomer chromophore during these titrations allowed us to determine the K_T and EM values. Furthermore, when this mononucleoside competitor is equipped with the BODIPY energy acceptor pair, fluorescence spectroscopy analysis additionally allowed us to monitor and quantify peripheral interactions between intact macrocycles and mononucleosides. Our results indicate that donor fluorescence deactivation during the competition titrations is due to binding of the complementary acceptor to both the product (cyclic tetramer) and reactant (monomer) sides of the macrocyclization reaction. These effects are more clearly discerned and quantified in the case of ***c*GdC$_4$**, due to its higher stability and stronger chelate cooperativity when compared to ***c*AdU$_4$**. At a moderate competitor content, associative processes may become dominant and the macrocycle acts as a host for the competitor. As the competitor ratio increases, the cyclic species is however forced to dissociate.

We deem that the outcome and conclusions of our work can be very interesting for the study of host–guest ensembles in which the host is a self-assembled system that can either dissociate or accommodate the guest molecule. Future work involving related complementary donor–acceptor FRET pairs will be focused on selecting guests with H-bonding motifs that can bind to specific sites of the macrocycle's periphery with high K_p association constants, and on utilizing the exceptional time resolution of fluorescence spectroscopy to monitor exchange kinetics between diverse components in these H-bonded macrocycles.

Conflicts of interest

There are no conflicts to declare.

Acknowledgements

Funding from the European Research Council (ERC-Starting Grant 279548 PROGRAM-NANO) and MINECO (CTQ2014-57729 P and CTQ2017-84727 P) is gratefully acknowledged. E. F. would like to thank Sharif University of Technology of Iran for financial support. D. S.-M. would like to acknowledge Comunidad de Madrid for financial support through contract PEJ16/IND/AI-0849.

Notes and references

1 C. A. Schalley, *Analytical Methods in Supramolecular Chemistry*, Wiley-VCH, Weinheim, 2012.
2 (*a*) K. E. Sapsford, L. Berti and I. L. Medintz, *Angew. Chem., Int. Ed.*, 2006, **45**, 4562–4588; (*b*) *FRET - Förster Resonance Energy Transfer: From Theory to Applications*, ed. I. Medintz and N. Hildebrandt, Wiley-VCH, Weinheim, 2014.
3 (*a*) S. Saini, G. Srinivas and B. Bagchi, *J. Phys. Chem. B*, 2009, **113**, 1817–1832; (*b*) H. Sahoo, *J. Photochem. Photobiol., C*, 2011, **12**, 20–30.

4 E. A. Jares-Erijman and T. M. Jovin, *Nat. Biotechnol.*, 2003, **21**, 1387–1395.
5 S. Preus and L. M. Wilhelmsson, *ChemBioChem*, 2012, **13**, 1990–2001.
6 (*a*) J. P. S. Farinha, J. G. Spiro and M. A. Winnik, *J. Phys. Chem. B*, 2001, **105**, 4879–4888; (*b*) M. Sustarsic and A. N. Kapanidis, *Curr. Opin. Struct. Biol.*, 2015, **34**, 52–59; (*c*) D. Shrestha, A. Jenei, P. Nagy, G. Vereb and J. Szöllősi, *Int. J. Mol. Sci.*, 2015, **16**, 6718–6756.
7 (*a*) R. K. Castellano, S. L. Craig, C. Nuckolls and J. Rebek Jr, *J. Am. Chem. Soc.*, 2000, **122**, 7876–7882; (*b*) E. S. Barrett, T. J. Dale and J. Rebek Jr, *J. Am. Chem. Soc.*, 2007, **129**, 3818–3819; (*c*) E. S. Barrett, T. J. Dale and J. Rebek Jr, *J. Am. Chem. Soc.*, 2007, **129**, 8818–8824.
8 V. A. Azov, A. Schlegel and F. Diederich, *Angew. Chem., Int. Ed.*, 2005, **44**, 4635–4638.
9 R. J. Brea, M. E. Vázquez, M. Mosquera, L. Castedo and J. R. Granja, *J. Am. Chem. Soc.*, 2007, **129**, 1653–1657.
10 (*a*) J. M. Rivera, M. Martín-Hidalgo and J. C. Rivera-Ríos, *Org. Biomol. Chem.*, 2012, **10**, 7562–7565; (*b*) F. Pu, L. Wu, X. Ran, J. Ren and X. Qu, *Angew. Chem., Int. Ed.*, 2015, **54**, 892–896.
11 (*a*) L. Zhang, Y. Wu and L. Brunsveld, *Angew. Chem., Int. Ed.*, 2007, **46**, 1798–1802; (*b*) A. Bill, H. Blockus, D. Stumpfe, J. Bajorath, A. Schmitz and M. Famulok, *J. Am. Chem. Soc.*, 2011, **133**, 8372–8379.
12 (*a*) M. Suresh, A. K. Mandal, E. Suresh and A. Das, *Chem. Sci.*, 2013, **4**, 2380–2386; (*b*) A. K. Mandal, M. Gangopadhyay and A. Das, *Chem. Soc. Rev.*, 2015, **44**, 663–676; (*c*) M. Gangopadhyay, A. Maity, A. Dey and A. Das, *J. Org. Chem.*, 2016, **81**, 8977–8987.
13 S. A. Denisov, Q. Gan, X. Wang, L. Scarpantonio, Y. Ferrand, B. Kauffmann, G. Jonusauskas, I. Huc and N. D. McClenaghan, *Angew. Chem., Int. Ed.*, 2016, **55**, 1328–1333.
14 C.-B. Huang, L. Xu, J.-L. Zhu, Y.-X. Wang, B. Sun, X. Li and H.-B. Yang, *J. Am. Chem. Soc.*, 2017, **139**, 9459–9462.
15 (*a*) S. Jiwpanich, J.-H. Ryu, S. Bickerton and S. Thayumanavan, *J. Am. Chem. Soc.*, 2010, **132**, 10683–10685; (*b*) L. Li and S. Thayumanavan, *Langmuir*, 2014, **30**, 12384–12390; (*c*) B. Gong, B.-K. Choi, J.-Y. Kim, D. Shetty, Y. H. Ko, N. Selvapalam, N. K. Lee and K. Kim, *J. Am. Chem. Soc.*, 2015, **137**, 8908–8911; (*d*) M. Zhang, X. Yin, T. Tian, Y. Liang, W. Li, Y. Lan, J. Li, M. Zhou, Y. Ju and G. Li, *Chem. Commun.*, 2015, **51**, 10210–10213.
16 L.-B. Meng, D. Li, S. Xiong, X.-Y. Hu, L. Wang and G. Li, *Chem. Commun.*, 2015, **51**, 4643–4646.
17 (*a*) K. Petkau-Milroy, D. A. Uhlenheuer, A. J. H. Spiering, J. A. J. M. Vekemans and L. Brunsveld, *Chem. Sci.*, 2013, **4**, 2886–2891; (*b*) T. Sendai, S. Biswas and T. Aida, *J. Am. Chem. Soc.*, 2013, **135**, 11509–11512; (*c*) L. Albertazzi, N. van der Veeken, M. B. Baker, A. R. A. Palmans and E. W. Meijer, *Chem. Commun.*, 2015, **51**, 16166–16168; (*d*) M. B. Baker, R. P. J. Gosens, L. Albertazzi, N. M. Matsumoto, A. R. A. Palmans and E. W. Meijer, *ChemBioChem*, 2016, **17**, 207–213; (*e*) A. Sarkar, S. Dhiman, A. Chalishazar and S. J. George, *Angew. Chem., Int. Ed.*, 2017, **56**, 13767–13771.
18 (*a*) T. F. A. De Greef, M. M. J. Smulders, M. Wolffs, A. P. H. J. Schenning, R. P. Sijbesma and E. W. Meijer, *Chem. Rev.*, 2009, **109**, 5687–5754; (*b*) J. D. Fox and S. J. Rowan, *Macromolecules*, 2009, **42**, 6823–6835; (*c*) C. Kulkarni, S. Balasubramanian and S. J. George, *ChemPhysChem*, 2013, **14**, 661–673; (*d*) F. Aparicio, F. Garcia and L. Sanchez, *Supramolecular Polymers in Encyclopedia of Polymer Science and Technology*, John Wiley & Sons, Inc., 2012, ISBN 9780471440260.
19 (*a*) C. A. Hunter and H. L. Anderson, *Angew. Chem., Int. Ed.*, 2009, **48**, 7488–7499; (*b*) G. Ercolani and L. Schiaffino, *Angew. Chem., Int. Ed.*, 2011, **50**, 1762–1768; (*c*) M. J. Mayoral, N. Bilbao and D. González-Rodríguez, *ChemistryOpen*, 2016, **5**, 10–32; (*d*) S. Di Stefano and G. Ercolani, Equilibrium Effective Molarity as a Key Concept in Ring-Chain Equilibria, Dynamic Combinatorial Chemistry, *Cooperativity and Self-assembly in Advances in Physical Organic Chemistry*, ed. I. H. Williams and N. H. Williams, Elsevier Ltd., 2016, vol. 50, ch. 1, pp. 1–77; (*e*) P. Motloch and C. A. Hunter, *Thermodynamic Effective Molarities for Supramolecular Complexes in Advances in Physical Organic Chemistry*, ed. I. H. Williams and N. H. Williams, Elsevier Ltd., 2016, vol. 50, ch. 2, pp. 77–118.
20 N. Bilbao, I. Destoop, S. De Feyter and D. González-Rodríguez, *Angew. Chem., Int. Ed.*, 2016, **55**, 659–663.
21 (*a*) C. Montoro-García, J. Camacho-García, A. M. López-Pérez, N. Bilbao, S. Romero-Pérez, M. J. Mayoral and D. González-Rodríguez, *Angew. Chem., Int. Ed.*, 2015, **54**, 6780–6784; (*b*) S. Romero-Pérez, J. Camacho-García, C. Montoro-García, A. M. López-Pérez, A. Sanz, M. J. Mayoral and D. González-Rodríguez, *Org. Lett.*, 2015, **17**, 2664–2667; (*c*) C. Montoro-García, J. Camacho-García, A. M. López-Pérez, M. J. Mayoral, N. Bilbao and D. González-Rodríguez, *Angew. Chem., Int. Ed.*, 2016, **55**, 223–227; (*d*) C. Montoro-García, M. J. Mayoral, R. Chamorro and D. González-Rodríguez, *Angew. Chem., Int. Ed.*, 2017, **56**, 15649–15653; (*e*) C. Montoro-García, N. Bilbao, I. M. Tsagri, F. Zaccaria, M. J. Mayoral, C. Fonseca Guerra and D. González-Rodríguez, *Chem.–Eur. J.*, 2018, **24**, 11983–11991.
22 M. J. Mayoral, C. Montoro-García and D. González-Rodríguez, *Self-assembled Systems via Nucleobase Pairing in Reference Module in Chemistry, Molecular Sciences and Chemical Engineering, Comprehensive Supramolecular Chemistry II*, ed. J. Atwood, Elsevier Ltd., 2017, pp. 191–257.
23 H. Yao, L. Ye, H. Zhang, S. Li, S. Zhang and J. Hou, *Chem. Rev.*, 2016, **116**, 7397–7457.
24 (*a*) A. Loudet and K. Burgess, *Chem. Rev.*, 2007, **107**, 4891–4932; (*b*) G. Ulrich, R. Ziessel and A. Harriman, *Angew. Chem., Int. Ed.*, 2008, **47**, 1184–1201; (*c*) D. Frath, J. Massue, G. Ulrich and R. Ziessel, *Angew. Chem., Int. Ed.*, 2014, **53**, 2290–2310.
25 M. J. Mayoral, J. Camacho-García, E. Magdalena-Estirado, M. Blanco-Lomas, F. Fadaei, C. Montoro-García, D. Serrano-Molina and D. González-Rodríguez, *Org. Biomol. Chem.*, 2017, **15**, 7558–7565.

26 J. Camacho-García, C. Montoro-García, A. M. López-Pérez, N. Bilbao, S. Romero-Pérez and D. González-Rodríguez, *Org. Biomol. Chem.*, 2015, **13**, 4506–4513.

27 These dye-conjugated molecules could be instead dissolved in $CDCl_3$, revealing relatively sharp peaks, and subjected to DOSY experiments in this solvent (see Fig. S1†). The diffusion coefficients obtained were used to estimate the cyclic tetramer size, which is in agreement with computational models. The gradual addition of DMSO-d_6 to these solutions resulted in cyclic tetramer dissociation, and the monomer could be detected in slow exchange with the cycle both in ^{1}H NMR and DOSY measurements (see Fig. S1† and our previous work).

28 Calculated using ReactLab™ EQUILIBRIA (Jplus Consulting Pty Ltd). This software offers the possibility of global fitting, meaning that all wavelengths in the whole spectra are fitted simultaneously (see the ESI†).

29 (*a*) H. Sun, C. A. Hunter, C. Navarro and S. Turega, *J. Am. Chem. Soc.*, 2013, **135**, 13129–13141; (*b*) S. Henkel, M. C. Misuraca, Y. Ding, M. Guitet and C. A. Hunter, *J. Am. Chem. Soc.*, 2017, **139**, 6675–6681.

30 *The speciation profiles were simulated by Hyss (Hyperquad Simulation and Speciation) version 4.0.31.*, http://www.hyperquad.co.uk/hyss.htm; L. Alderighi, P. Gans, A. Lenco, D. Peters, A. Sabatini and A. Vacca, *Coord. Chem. Rev.*, 1999, **184**, 311–318.

31 This is not the ideal situation for the titration experiments monitored by fluorescence spectroscopy, since it is preferable to excite the donor and monitor its emission quenching at a constant donor concentration, while using the acceptor as the titration agent added in excess (that is, the **GdC** + **aC** and **AdU** + **aU** combination detailed in the manuscript). In the alternative titration (**GaC** + **dC** or **AaU** + **dU**), in contrast, the donor concentration is constantly increasing and this brings about several practical inconveniences. However, the opposite occurs when considering CD spectroscopy. In the regular titration (**GdC** + **aC** and **AdU** + **aU**), the absorbance of excess **aC**/**aU** in the 300–500 nm region quickly saturates the absorption spectrum and hampers a correct monitoring of the ***c*GdC$_4$**/***c*AdU$_4$** CD signal (see Fig. S3E†). Instead, ***c*GaC$_4$** and ***c*AaU$_4$** macrocycles show isolated CD signals between 500 and 700 nm, a region where the absorption of the donor molecules does not interfere (or at least not up to a reasonable excess, see Fig. 6 and S3F†).